Interdisciplinary Research in Medical Sciences Specialty
ISSN: 3062-4401
2025, Volume 5, Issue 2, Page No: 279-300
Copyright CC BY-NC-SA 4.0
Available online at: www.galaxypub.co/page/journals

Galaxy Publication

Exosomal YES1 from Osteosarcoma Cells Drives Malignant Progression through the ERK/MAPK Pathway

Wei Zhang[1]*, Chen Hui[2], Michael Tan[1]

[1]Department of Sarcoma Biology and Exosome Signaling, Faculty of Medicine, University of Melbourne, Melbourne, Australia.
[2]Department of Oncogenic Signaling and ERK/MAPK Pathway, Faculty of Medicine, National University of Singapore, Singapore.

***E-mail** ✉ wei.zhang@unimelb.edu.au

Received: 16 October 2025; **Revised:** 22 December 2025; **Accepted:** 26 December 2025

ABSTRACT

Osteosarcoma (OS) represents the predominant primary malignant bone tumor among children and young adults and continues to present major therapeutic obstacles. This investigation explored the involvement of exosomes, which serve as critical mediators of cell-to-cell signaling, in driving OS advancement and pinpointed promising therapeutic candidates. Experiments performed in both in vitro cellular systems and in vivo animal models revealed that exosomes secreted by OS cells substantially accelerated tumor cell proliferation, motility, and invasive capacity. Proteomic profiling through data-independent acquisition mass spectrometry demonstrated prominent enrichment of the proto-oncogene tyrosine-protein kinase YES1 within OS-derived exosomes. Comprehensive bioinformatics evaluation combined with clinical data analysis established that YES1 exhibits elevated expression in various malignancies and is linked to unfavorable patient outcomes. In OS, increased YES1 levels were specifically associated with diminished overall survival and more adverse prognostic features. Quantitative PCR, Western blot, and immunohistochemistry (IHC) analyses of patient-derived samples confirmed markedly higher YES1 abundance in OS tissues than in corresponding normal tissues. Functional mechanistic experiments utilizing YES1 silencing (shYES1) and forced expression (OE YES1) constructs, alongside exosome treatment and pharmacological pathway modulators, identified ERK phosphorylation as a key mediator of YES1-induced oncogenic properties. shYES1 cells exhibited pronounced suppression of proliferation, migration, and invasion, which was partly restored upon exosome addition and further diminished by MAPK pathway inhibition. Conversely, OE YES1 cells displayed strongly augmented malignant traits that were intensified by exosomes and additionally enhanced through MAPK pathway stimulation. Supporting Western blot data showed lowered phosphorylation of MEK and ERK, accompanied by elevated phosphorylation of p38 and JNK in YES1-depleted cells, with inverse patterns in the overexpression setting. These shifts in phosphorylation status were counteracted or lessened by EGF/IL-1β stimulation or U0126/SB-203580 application, respectively, while total levels of MEK, JNK, p38, and ERK proteins remained stable. Multiplex IHC further substantiated bioinformatics predictions by revealing a strong association between YES1 expression and immune-associated pathways within OS specimens. Overall, the results emphasize the central contribution of exosomal YES1 to OS development and its interplay with tumor immunology, underscoring its potential value as both a prognostic biomarker and a viable therapeutic target. This research elucidates the mechanisms through which YES1 influences malignant behavior and immune regulation, thereby contributing fresh perspectives toward enhancing clinical management and outcomes for OS patients.

Keywords: Exosomal YES1, Immune cell infiltration, MAPK signaling pathway, Osteosarcoma, Tumor microenvironment

How to Cite This Article: Zhang W, Hui C, Tan M. Exosomal YES1 from Osteosarcoma Cells Drives Malignant Progression through the ERK/MAPK Pathway. Interdiscip Res Med Sci Spec. 2025;5(2):279-300. https://doi.org/10.51847/rF6JmtDInH

Introduction

Epidemiological data consistently designate osteosarcoma (OS) as the most frequent primary malignant neoplasm of bone, primarily impacting pediatric and adolescent populations. This aggressive malignancy carries a 5-year

© 2025 Interdisciplinary Research in Medical Sciences Specialty

overall survival rate of roughly 70% [1-3]. Metastatic disease is detectable at diagnosis in approximately 15%–20% of cases, with pulmonary sites representing the most frequent location of distant spread. Current standard management combines systemic chemotherapy and radiotherapy with surgical intervention, typically involving limb salvage procedures or, less commonly, amputation. Despite these approaches, therapeutic options remain constrained by the absence of well-defined molecular targets. Hence, the identification of innovative molecular targets constitutes an urgent priority in ongoing OS research [4].

Mounting evidence highlights extensive crosstalk between heterogeneous cell types within the tumor microenvironment (TME) and neoplastic cells across all phases of tumor initiation and advancement [5-7]. Numerous reports underscore the fundamental importance of extracellular vesicles (EVs) in facilitating intercellular communication under both homeostatic and pathological conditions [8]. Exosomes constitute a specialized category of EVs, ranging from 50 to 150 nm in size, and are abundantly present in diverse bodily fluids including culture media, plasma, and urine. These vesicles transport a complex payload of proteins, metabolites, and genetic material encompassing DNA and RNA [9, 10]. Accumulating findings demonstrate that neoplastic cells actively secrete exosomes that foster tumor growth and dissemination [11]. Exosomal proteins, in particular, exert significant influence on tumor biology; fluctuations in their expression profiles and mutational status are intimately connected with cancer initiation, progression, metastatic spread, and resistance to treatment [12, 13]. Moreover, proteins packaged within tumor-derived exosomes can reprogram immune cells, enabling malignant cells to circumvent immune detection and elimination within the TME [12, 14, 15]. Such attributes position exosomal proteins as attractive candidates for novel biomarkers and therapeutic intervention in OS. Consequently, systematic examination of the exosomal proteome in OS is vital for uncovering the molecular underpinnings of disease progression.

High-resolution mass spectrometry (MS)-driven proteomic strategies have gained widespread adoption for the discovery of disease-specific biomarkers and actionable therapeutic targets, owing to their exceptional sensitivity in quantifying low-abundance proteins across broad concentration ranges [16-18]. This platform has been successfully deployed in multiple cancer investigations to reveal previously unrecognized biomarkers and treatment vulnerabilities [19]. In the current work, we applied data-independent acquisition mass spectrometry (DIA-MS, Orbitrap Exploris 480, Thermo Fisher) to compare exosomal proteomes isolated from normal osteoblasts and OS cell lines, aiming to uncover distinctive OS-associated markers. Exosomes harvested from the OS lines MNNG/HOS and SaOS-2, together with control osteoblastic cells, were subjected to proteomic analysis. Several proteins uniquely enriched in tumor-derived exosomes emerged as candidate biomarkers. Among these, exosomal YES1 stood out; subsequent bioinformatics interrogation and functional validation through cell-based and animal studies established its regulatory effects on key oncogenic processes including proliferation, invasion, migration, and metastatic potential.

YES1 is a non-receptor tyrosine kinase encoded by the YES1 gene mapped to chromosome 18p11.32 and belongs to the Src family kinases (SFKs). These kinases modulate an array of downstream cascades such as EGFR, PI3K/Akt, and Ras/MAPK pathways, thereby participating in the control of cellular proliferation, survival, differentiation, motility, invasion, adhesion, angiogenesis, and immune modulation [20-22]. Growing attention has focused on YES1 as a prospective anticancer target given its contributions to proliferation, differentiation, and programmed cell death. These activities implicate YES1 in both normal physiology and disease states, notably cancer development and acquired drug resistance. Nonetheless, the precise mechanisms whereby exosomal YES1 accelerates tumor progression and coordinates communication between cancer cells and the surrounding TME require further elucidation.

In conclusion, by combining DIA-MS exosomal proteomics with bioinformatics, functional experimentation, and clinical corroboration, the present study has delineated a novel panel of candidate biomarkers and therapeutic targets for OS. The incorporation of YES1 into OS-derived exosomes was validated, and its active role in fueling disease progression was delineated, yielding important mechanistic insights and supporting its development as a clinically relevant target.

Materials and Methods

Patient samples

The present investigation included specimens from 44 individuals with primary osteosarcoma (OS) who had undergone radical resection surgery at Shanghai Tongji Hospital, Shanghai Tenth People's Hospital, and Shanghai

First People's Hospital during the period spanning 2010 to 2019. None of these patients had been subjected to neoadjuvant radiotherapy or chemotherapy. YES1 protein abundance was evaluated by immunohistochemistry (IHC) in 24 OS tissue samples paired with adjacent non-malignant tissues. Within the cohort, 21 patients (47.72%) were male, with a mean age of 22.86 ± 9.23 years, and 23 patients (52.28%) were female, with a mean age of 18.70 ± 6.88 years. Matched tumor and non-tumor tissue pairs were additionally procured to determine YES1 protein levels via western blot analysis and to quantify YES1 mRNA expression using qRT-PCR. Approval for the study was granted by the institutional Ethics Committee, and informed consent was secured in written form from every participant prior to inclusion.

Cell culture and transfection

The human osteoblastic cell line hFOB 1.19 along with the OS cell lines MNNG/HOS, SaOS-2, and 143B were sourced from the American Type Culture Collection (Shanghai). Culture of hFOB 1.19 cells was performed in Dulbecco's modified Eagle's medium/F12 (DMEM/F12, Gibco) enriched with 10% fetal bovine serum (FBS, HyClone) and 0.6 mg/mL G-418 sulfate (Solarbio) at 33.5°C. The OS cell lines MNNG/HOS, SaOS-2, and 143B were propagated in DMEM supplemented with 10% FBS under standard conditions of 37°C and 5% CO_2 in a humidified incubator. All media additionally contained 100 U/mL penicillin G and 100 μg/mL streptomycin sulfate. For genetic manipulation, 3×10^5 OS cells were seeded per well in six-well plates and allowed to attach for 12 h. Transfection was subsequently executed with Lipofectamine™ 3000 reagent (Thermo Fisher Scientific) as directed by the supplier. Constructs including short hairpin RNAs directed against YES1 (sh#1/2/3), the matched negative control (sh-NC), the YES1 overexpression plasmid pcDNA3.1-YES1, and corresponding empty vectors were supplied by WZ Biosciences Inc.

Isolation and identification of exosomes

Exosomes originating from human osteoblasts (hFOB 1.19-Exos) and from the OS cell lines MNNG/HOS, SaOS-2, and 143B were prepared following a well-established differential ultracentrifugation procedure. When cultures achieved roughly 60% confluence, cells were washed thrice with phosphate-buffered saline (PBS) before switching to medium containing 10% exosome-depleted FBS (absin, #abs993, Shanghai). Conditioned medium was collected after 48 h and sequentially centrifuged at 300g for 10 min, 3000g for 30 min, and 10,000g for 60 min, all at 4°C. The cleared supernatant underwent ultracentrifugation at 100,000g for 70 min at 4°C. Pellets were resuspended in PBS, passed through a 0.22-μm Steritop™ filter (Millipore), and subjected to a further round of ultracentrifugation at 100,000g for 70 min. The resulting exosome pellets were resuspended in 50 μL sterile PBS and maintained at −80°C for downstream applications.

Transmission electron microscopy

Isolated exosomes were resuspended and fixed using 4% paraformaldehyde for 2 h. Droplets of the suspension were deposited onto Formvar carbon-coated 400-mesh copper grids and stabilized with 1% glutaraldehyde for 20 min. Negative staining was performed first with 2% uranyl-oxalate (pH 7.0) for 5 min, followed by 10 min in a 9:1 combination of 2% methylcellulose (pH 4.0) and 4% uranyl acetate. Grids were air-dried, and images were captured on a Thermo-Fisher transmission electron microscope operating at 80 kV. Particle diameters were subsequently measured employing ImageJ software (ImageJ v2.1.4.7, National Institutes of Health).

Nanoparticle tracking analysis

The concentration and size profile of purified exosomes were characterized by nanoparticle tracking analysis (NTA) on a NanoSight platform (Malvern Instruments) equipped with a 405 nm laser. Raw data were processed using NTA 3.0 software. Hydrodynamic diameters were derived from the Stokes-Einstein equation: $D = kT/6\pi\eta r$ (where D denotes the diffusion coefficient, k is Boltzmann's constant, T represents absolute temperature, r is the particle radius, and η is the viscosity of the dispersion medium).

Western blotting

Whole-cell lysates or exosomal preparations were generated in RIPA lysis buffer containing protease and phosphatase inhibitor cocktails. Proteins were resolved by SDS-PAGE and electrotransferred onto polyvinylidene difluoride membranes (Millipore). Following blockade in 5% non-fat milk for 1 h, membranes were probed overnight at 4°C with primary antibodies against: Alix, TSG101, HSP70, CD9, and GM130 (Abcam, #ab275377,

#ab125011, #ab181606, #ab263019, #ab52649, all at 1:1000), β-actin (Abcam, #ab92486, 1:1000), YES1 (Abmart, #T58388, 1:1000), ERK1/2 (Proteintech, #11257, 1:1000), p-ERK1/2 (Proteintech, #28733, 1:1000), MEK (Proteintech, #11049, 1:1000), p-MEK (Proteintech, #28930, 1:1000), p38 (Proteintech, #14064, 1:1000), p-p38 (Proteintech, #28796, 1:1000), JNK (Proteintech, #66210, 1:1000), p-JNK (Proteintech, #80024, 1:1000), and GAPDH (Proteintech, #60004, 1:5000). After incubation with species-appropriate secondary antibodies for 1 h at ambient temperature, signals were developed using an enhanced chemiluminescence detection system (Millipore).

Exosome labeling and tracing

Exosomes harvested from culture supernatants were labeled with the lipophilic fluorescent dye 3,3′-dioctadecyloxacarbocyanine perchlorate (DiO) (Beyotime, #C1038), while recipient cells were counterstained with phalloidin (Beyotime, #C2207S) in accordance with a prior established method. Labeled exosomes were then added to OS cell cultures to track internalization. Uptake was monitored and documented by fluorescence microscopy following incubation intervals of 0, 12, and 24 h at 37°C.

Mass spectrometry based on data-independent acquisition

Protein extraction

Individual exosome samples were pulverized in liquid nitrogen prior to lysis in SDT buffer (containing 4% SDS, 100 mM DTT, and 10 mM TEAB). The mixture underwent ultrasonication on ice for 5 min, after which it was incubated at 95°C for 8 min and centrifuged at 12,000g for 15 min at 4°C. Alkylation of the supernatant was achieved by adding iodoacetamide and incubating for 1 h at room temperature in darkness. A second centrifugation at 12,000g for 15 min at 4°C was performed, the resulting precipitate was harvested and rinsed with 1 mL cold acetone. The final pellet was resuspended in dissolution buffer (8 M urea, 100 mM TEAB, pH 8.5).

LC-MS/MS analysis in DDA mode

Shotgun proteomic profiling for spectral library generation was executed in data-dependent acquisition (DDA) mode on an EASY-nLC™ 1200 UHPLC system (Thermo Fisher) interfaced with a Q Exactive™ HF-X mass spectrometer (Thermo Fisher). Each injection consisted of 4 μg of fractionated supernatant supplemented with 0.8 μL of indexed retention time (iRT) reagent. Peptides were initially trapped on a laboratory-packed C18 Nano-Trap column (4.5 cm × 75 μm, 3 μm) and subsequently separated on a custom analytical column (25 cm × 150 μm, 1.9 μm). Ionization occurred via an electrospray source (Nanospray Flex™, Thermo Fisher) operated at 2.1 kV spray voltage and 320°C capillary temperature. Survey scans were acquired with an AGC target of 3×10^6, maximum injection time of 80 ms, m/z range of 350–1500, and resolution set at 120,000 (at m/z 200). The top 40 precursor ions were isolated for fragmentation by higher-energy collisional dissociation, with MS/MS spectra recorded at 15,000 resolution (at m/z 200). Additional MS/MS settings comprised an AGC target of 5×10^4, maximum injection time of 45 ms, normalized collision energy of 27%, intensity threshold of 1.1×10^4, and dynamic exclusion of 20 s. Acquired raw files were stored in ".raw" format for subsequent DDA library construction.

Protein identification and quantitation

Processing of both identification and quantitation data, along with DIA visualization, was conducted in Proteome Discoverer 2.2 (PD 2.2, Thermo Scientific). Database searching parameters included a precursor tolerance of 10 ppm and fragment tolerance of 0.02 Da. Fixed modification was set to carbamidomethylation of cysteine, while variable modifications encompassed methionine oxidation and N-terminal acetylation. A maximum of two missed tryptic cleavages was allowed. High-confidence peptide spectrum matches (PSMs) were retained at ≥99% confidence level. Proteins required identification by at least one unique peptide, and both PSMs and protein identifications were controlled at a false discovery rate (FDR) ≤ 1.0%. The resulting PD 2.2 files were transferred to Spectronaut software (version 14.0, Biognosys) to assemble a spectral library. Appropriate peptides and their corresponding fragment ions were chosen according to standard selection criteria to establish a Target List. Imported DIA raw data underwent targeted extraction of ion-pair chromatographic traces. Peptide identification and quantification relied on peak matching and area integration, with retention times aligned using iRT standards and a precursor Q-value filter of 0.01. Differential abundance testing between groups was performed via t-test.

Proteins displaying significant changes ($p < 0.05$ and $|\log_2 FC| > 1.5$) were classified as differentially expressed proteins (DEPs) [23, 24].

Functional analysis of proteins and differentially expressed proteins

Functional characterization was carried out using InterProScan to assign Gene Ontology (GO) terms and InterPro (IPR) domains by querying the non-redundant protein sequence collection, which integrates Pfam, PRINTS, ProDom, SMART, ProSite, and PANTHER databases. Additional classification into protein families and biological pathways was achieved through Clusters of Orthologous Groups and KEGG resources. For DEPs, comprehensive downstream investigations included volcano plot visualization, heatmap-based clustering, and enrichment testing across GO categories, IPR domains, and KEGG pathways. Potential physical and functional associations among proteins were mapped by querying the STRING-db database.

Bioinformatic analysis

Pan-cancer transcriptomic datasets were downloaded from the TCGA portal (https://portal.gdc.cancer.gov/). Matched normal samples were taken from non-cancerous adjacent tissues of the same individuals. Fold-change values were transformed to $\log_2$ scale, followed by GO term annotation and KEGG pathway enrichment using the "clusterProfiler" R package; graphical outputs were generated with "ggplot2". Source annotation databases included NCBI (http://www.ncbi.nlm.nih.gov/), UniProt (http://www.uniprot.org/), and the Gene Ontology resource (http://www.geneontology.org/). TCGA pan-cancer mutation data were further analyzed to determine tumor mutational burden (TMB) and microsatellite instability (MSI), defined respectively as somatic mutations per megabase and the rate of insertions/deletions within microsatellite regions [24-26]. Associations between YES1 expression and TMB or MSI were evaluated by Spearman rank correlation.

Assessment and correlation of immune cell infiltration in relation to YES1 expression levels

The tumor immune microenvironment encompasses a complex mixture of immune and inflammatory cells, fibroblasts, stromal elements, and secreted cytokines/chemokines that collectively modulate disease development. Evaluation of immune infiltration patterns therefore holds substantial value for prognostic assessment and therapeutic guidance. To explore links between YES1 expression and immune contexture, the "immuneeconv" R package was employed to apply several established deconvolution methods: CIBERSORT, EPIC, MCPCOUNTER, QUANTISEQ, TIMER, and XCELL. Infiltration abundances were estimated for a broad panel of immune populations, including naive B cells, resting and activated memory $CD4^+$ T cells, $CD8^+$ T cells, T follicular helper cells, regulatory T cells (Tregs), γδ T cells, monocytes, natural killer cells, M0/M1/M2-polarized macrophages, neutrophils, eosinophils, activated and resting mast cells, and dendritic cells. Results were visualized using the R packages "ggplot2," "ggpubr," and "ggExtra," applying a stringent significance cutoff of $p < 0.001$.

Functional assays

Cell proliferation EdU assay

Cell proliferative activity was determined using the kFluor555-EdU cell proliferation detection kit (Keygen Biotechnology, #KGA337) in accordance with the manufacturer's guidelines. In short, MNNG/HOS and SAOS-2 cells (3×10^3 cells/well) were exposed to either PBS or exosomes for 24 h, plated into 96-well plates (Corning), and then labeled with 50 μM EdU at 37°C in a 5% CO_2 atmosphere for 4 h. Cells were subsequently fixed with 4% paraformaldehyde for 20 min at 37°C, incubated with the kFluor555 reaction mixture for 30 min, and counterstained using Hoechst 33342. Fluorescent images were acquired, and the percentage of EdU-positive cells was measured with ImageJ software.

Wound healing assay

MNNG/HOS and SAOS-2 cells were plated at 2×10^5 cells per well in 6-well plates (Corning) and pretreated with PBS or exosomes for 24 h. A uniform scratch was generated in the cell monolayer using a sterile 200 μL pipette tip, followed by two washes with 1× PBS to clear detached cells. Wound closure was observed and photographed at 100× magnification under a Nikon Inverted Research Microscope Eclipse Ti at 0, 24, and 48 h after wounding. Identical microscopic fields were recorded at each interval to ensure reliable comparison of migration rates.

Cell apoptosis analysis

Cells were seeded at 5×10^5 cells per well in six-well plates and pretreated with PBS or exosomes for 24 h. After treatment, cells were collected by centrifugation at 300g for 5 min and washed three times with 1× PBS. The cell suspension was then incubated with 5 μL FITC-Annexin V and 5 μL propidium iodide (PI) for 10 min at 37°C protected from light. Apoptotic cell populations were analyzed on a BD FACS Aria II flow cytometer (BD Biosciences).

Transwell assay

Migration and invasion abilities were assessed using 24-well Transwell inserts containing 8 μm polycarbonate membranes (Millipore). For the invasion assay, membranes were coated with 500 ng/mL Matrigel solution (BD Biosciences) and incubated for 4 h at room temperature. The lower compartment was filled with 500 μL medium containing 10% FBS, while 1×10^5 cells in 200 μL serum-free medium were placed in the upper compartment. Following incubation, cells that had penetrated the membrane were fixed with methanol and stained with 0.5% crystal violet (Beyotime). Five randomly chosen fields per membrane were imaged and quantified using a Nikon Inverted Research Microscope Eclipse Ti. The migration assay was performed using the identical protocol except that Matrigel coating was omitted.

Quantitative real-time polymerase chain reaction

Paired osteosarcoma tissues were minced into small pieces of about 1 mm^3. Total RNA was extracted using TRIzol reagent (Invitrogen) and reverse-transcribed with the reverse transcription reagent (Takara Biotechnology, #RR036A) following the manufacturer's instructions. YES1 mRNA levels were quantified by qRT-PCR using gene-specific primers in three independent runs on an ABI 7500 real-time PCR system (Applied Biosystems), with GAPDH employed as the internal control. Relative gene expression was calculated using the $2^{-\Delta\Delta Ct}$ method.

Immunohistochemistry

YES1 protein expression in osteosarcoma tissues was evaluated by immunohistochemistry on paraffin-embedded sections utilizing an anti-YES1 antibody (Abmart, #T58388, dilution 1:100) according to a standardized procedure. Tissue slides were deparaffinized, rehydrated, and rinsed prior to endogenous peroxidase blocking and microwave-mediated antigen retrieval. After blocking nonspecific binding sites, sections were incubated with the primary antibody for 1 h at room temperature. Slides were then washed, treated with secondary antibody, HRP-streptavidin conjugate, and developed with 3,3-diaminobenzidine tetrahydrochloride. Counterstaining was performed with hematoxylin. The final IHC score for YES1 was obtained by multiplying staining intensity by the proportion of positively stained cells. Intensity grading was defined as 0 (negative), 0.5 (weakly positive), 1 (light yellow or light brown), and 2 (yellow or brown). The positive staining rate was calculated as the percentage of positively labeled cells among the total cell population. In parallel, multiplex immunofluorescence staining was conducted on separate sections using a multiplex fluorescent immunohistochemical staining kit (Absin, abs50015) with antibodies directed against YES1, CD4, FOXP3 (Abmart, #T58388, #T55392, #TA6544, 1:100), and PD-L1 (Abcam, #ab228415, 1:500), together with DAPI for nuclear visualization.

Establishment of in vivo tumor models

Four-week-old female and male nude mice were purchased and maintained in a specific pathogen-free environment with a 12-h light/dark cycle at the Hubei Laboratory Animal Centre of Tongji University, Shanghai, China. All procedures involving animals were performed in compliance with the institutional ethical guidelines of Tongji University. To establish xenograft tumors, 1×10^6 MNNG/HOS luciferase cells (pretreated with PBS or exosomes for 24 h) were subcutaneously injected into the subaxillary region of each mouse (n = 6 per group) to reach an initial tumor volume of approximately 60 mm^3. Tumor growth was monitored three weeks post-injection using the CRI Maestro™ non-invasive fluorescence imaging system. Prior to imaging, mice received anesthesia with ketamine (100 mg/kg) and xylazine (12 mg/kg). After imaging, animals were euthanized and tumors were harvested for further examination. Tumors excised at day 28 were fixed in 4% paraformaldehyde and paraffin-embedded. Sections of 3 μm thickness were prepared for subsequent histological studies. Deparaffinization was performed in xylene for 20 min, followed by rehydration through a graded ethanol series (5 min per step). H&E staining and TUNEL assays were applied to tumor and organ sections as recommended by

the manufacturers. Microscopic evaluation was carried out on a Nikon Eclipse Ti-U microscope (Nikon Corporation).

TUNEL assay

To determine the influence of exosomes on osteosarcoma progression, the extent of necrosis within tumor tissues was qualitatively evaluated by TUNEL staining performed according to a previously reported protocol (#G1507, Servicebio).

Statistical analysis

All experiments were conducted in triplicate, with results expressed as mean ± standard deviation (SD). Statistical evaluations were performed using the Statistical Package for the Social Sciences (SPSS, version 25.0). Group differences were analyzed by Student's t-test or the Mann–Whitney U test, as appropriate. Associations between variables were examined using Spearman's rank correlation. Statistical significance was defined as a p-value < 0.05. Graphical representations, such as heatmaps, volcano plots, and scatter plots, were created with the Heatmap package 2 and the ggplot2 package within the R programming environment. The Wilcoxon–Mann–Whitney test was applied for significance testing in the R software. Fisher's exact test was utilized to determine enriched GO terms, and p-values were adjusted for multiple testing using the false discovery rate (FDR) method.

Results and Discussion

Isolation and characterization of exosomes from osteoblasts and OS cells and assessment of their cellular uptake

Exosomes were obtained from the conditioned medium of osteoblasts, MNNG/HOS, and SaOS-2 cells via ultracentrifugation. Characterization was carried out using transmission electron microscopy (TEM), nanoparticle tracking analysis (NTA), and Western blotting. TEM images displayed the classic cup-like morphology with a distinct bilayer membrane, and the vesicles measured 80 to 150 nm in diameter on average, matching typical exosome properties described in the literature **(Figures 1a and 1b)**. Western blotting verified strong positivity for the exosome-specific proteins Alix, CD9, HSP70, and TSG101, whereas the non-exosomal marker GM130 was undetectable **(Figure 1c)**.

Uptake studies involved incubating DiO-labeled exosomes with OS cells (MNNG/HOS and SaOS-2). No fluorescence was observed at 0 h, but clear green cytoplasmic signals appeared after 12 h and became more intense at 24 h, demonstrating progressive time-dependent internalization by the recipient cells **(Figures 1d and 1e)**.

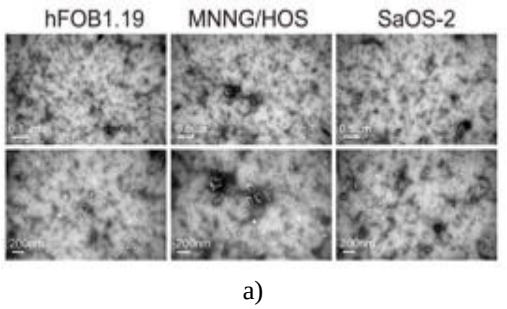

a)

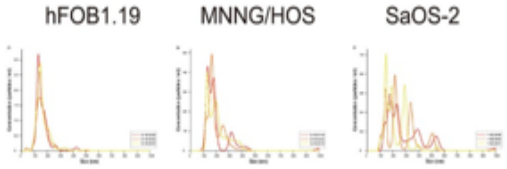

b)

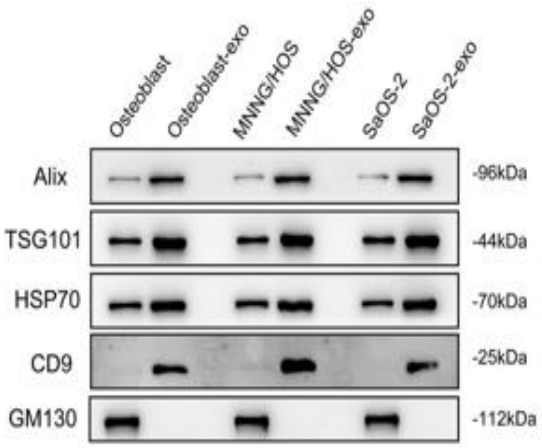

c)

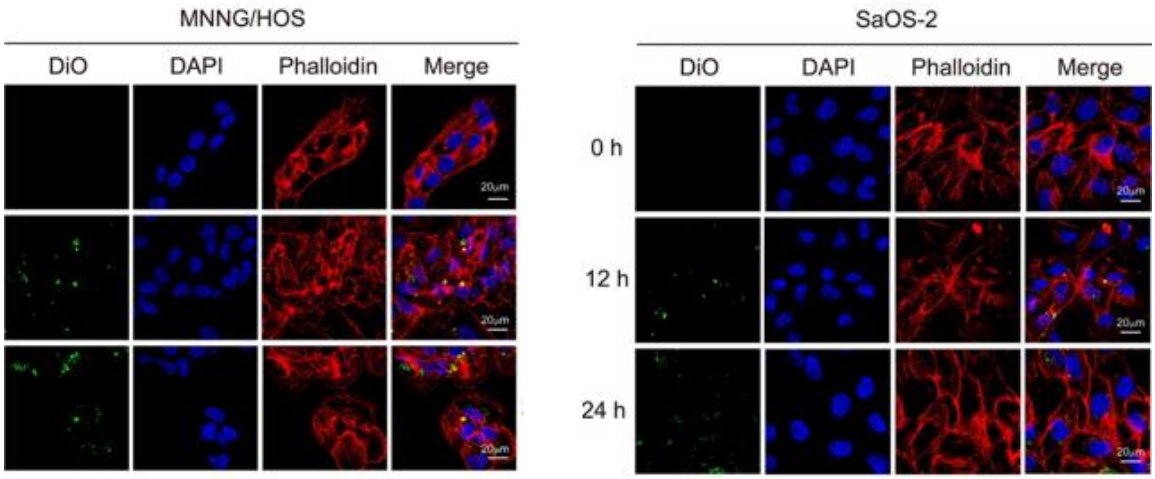

d) e)

Figure 1. Characterization of exosomes secreted by OS cells. (a) Exosomes isolated from culture supernatants of osteoblasts and OS cell lines were examined for morphology and size by transmission electron microscopy (upper scale bar = 0.5 μm, lower scale bar = 200 nm). (b) Size distribution profile of OS cell-derived exosomes determined by NTA. (c) Western blot detection of exosomal markers (Alix, TSG101, HSP70, CD9) and absence of GM130 in hFOB1.19-Exo, MNNG/HOS-Exo, and SaOS-2-Exo; whole-cell lysates from the corresponding cell lines served as positive controls. (d, e) Immunofluorescence analysis of DiO-labeled exosome internalization by MNNG/HOS and SaOS-2 cells at specified time points. Scale bar, 20 μm. NTA, nanoparticle tracking analysis; OS, osteosarcoma.

Exosomes from OS cells stimulate proliferation, migration, and invasion in OS cells

Prior research has linked tumor cell-derived exosomes closely with cancer development. In the present work, exosomes purified from MNNG/HOS and SaOS-2 culture supernatants were used to investigate their functional effects on OS progression. Multiple assays were employed to evaluate cellular responses. EdU incorporation assays showed that treatment with OS-derived exosomes led to a substantial rise in cell proliferation. Flow cytometry analysis indicated a notable decrease in apoptosis rates among exosome-exposed OS cells relative to untreated controls **(Figures 2a–2f)**. Wound-healing and Transwell chamber assays further demonstrated enhanced migratory and invasive behaviors following exosome treatment **(Figures 2h–2o)**.

These observations were extended to an in vivo xenograft model in nude mice. Animals inoculated with exosome-pretreated MNNG/HOS luciferase cells exhibited accelerated tumor expansion as measured by bioluminescence imaging. Histopathological evaluation with HE staining, PCNA immunohistochemistry, and TUNEL assay corroborated increased proliferative activity and reduced cell death in tumors from the exosome-treated group **(Figure 2p)**. In summary, results from both in vitro and in vivo models indicate that exosomes secreted by OS cells exert a strong stimulatory effect on OS cell proliferation, migration, and invasion.

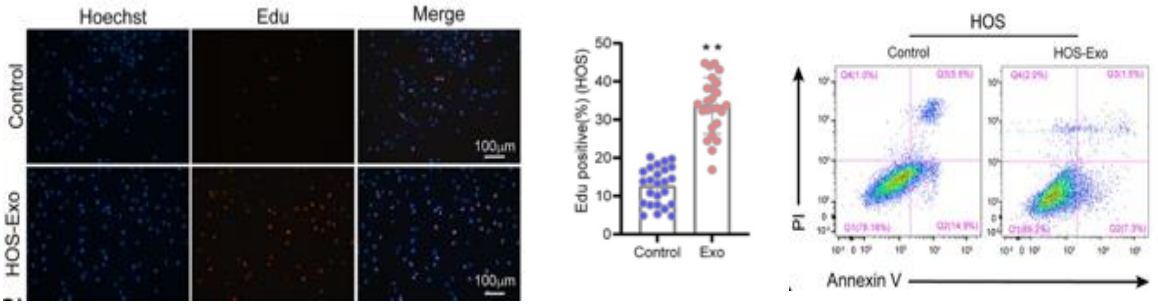

a) b) e)

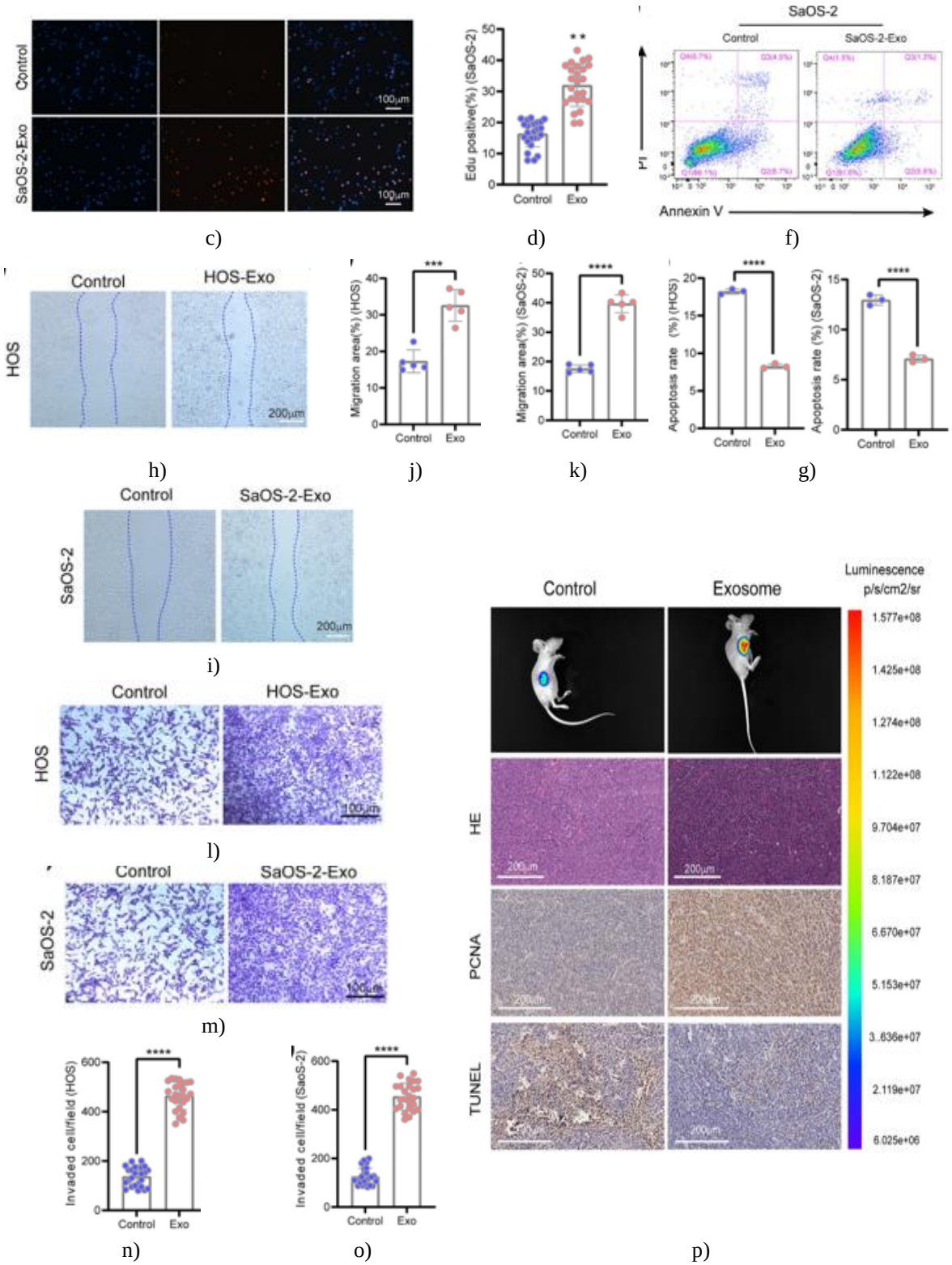

Figure 2. Impact of exosomes secreted by OS cells on malignant behaviors in OS cells. (a, b) EdU-based proliferation assessment in MNNG/HOS cells with or without exposure to OS cell-derived exosomes; (B) percentage of EdU-positive cells in control versus HOS-exo groups. n = 5. Scale bar, 100 μm. (c, d) EdU proliferation assay in SaOS-2 cells treated with or without OS-derived exosomes; quantification of EdU-positive cells in control and SaOS-2-exo groups. n = 5. Scale bar, 100 μm. (e–g) Flow cytometric detection of apoptosis using Annexin V/PI staining in (e) MNNG/HOS and (f) SaOS-2 cells; (g) summary of mean apoptosis percentages for both cell lines. n = 3. (h–k) Wound-healing images of (h) MNNG/HOS and (i) SaOS-2 cells at 0 h and 24 h; wound margins are marked by dotted lines. Graphs display the average wound closure rates for (j) MNNG/HOS and (k) SaOS-2 cells. n = 5; Scale bar, 200 μm. (l–p) Migration and

invasion analysis via Transwell and Matrigel-coated Transwell assays in (l) MNNG/HOS and (M) SaOS-2 cells. Quantitative results of migrated/invaded cells for (n) MNNG/HOS and (O) SaOS-2. n = 5. Scale bar, 200 μm. (p) Bioluminescence imaging of subcutaneous tumors formed by control or exosome-pretreated MNNG/HOS cells in nude mice (n = 6 per group). HE staining, PCNA IHC, and TUNEL assay images from the tumors are also shown. Scale bar, 200 μm. Data are expressed as mean ± SD of three independent experiments. Statistical significance was determined by two-tailed unpaired Student's t-test ($p < 0.05$, $p < 0.01$, $p < 0.001$). IHC, immunohistochemistry; OS, osteosarcoma; PCNA, proliferating cell nuclear antigen; TUNEL, terminal deoxynucleotidyl transferase-mediated dUTP-biotin nick end labeling.

Quantitative proteomic analysis

A spectral library was generated and examined using conventional data-dependent acquisition (DDA) mass spectrometry on exosomal proteins obtained from human osteoblasts and OS cell lines (MNNG/HOS, SaOS-2, and 143B). This involved four experimental groups comprising a total of 12 samples. The analysis led to the detection of more than 2000 proteins, yielding a detailed catalog of the exosomal proteome. Subsequent data acquisition was performed employing the data-independent acquisition (DIA) approach. Differential expression analysis was conducted with the MSstats package to determine fold changes and statistical significance. Proteins were classified as differentially expressed when they satisfied the criteria of log2(fold change) ≥ 1.5 and $p < 0.05$. Following the removal of duplicates and undetected entries, five genes consistently upregulated across the comparisons were identified: YES1, ITGA4, HIST1H4A, PSME1, and XPNPEP3 **(Figure 3a)**.

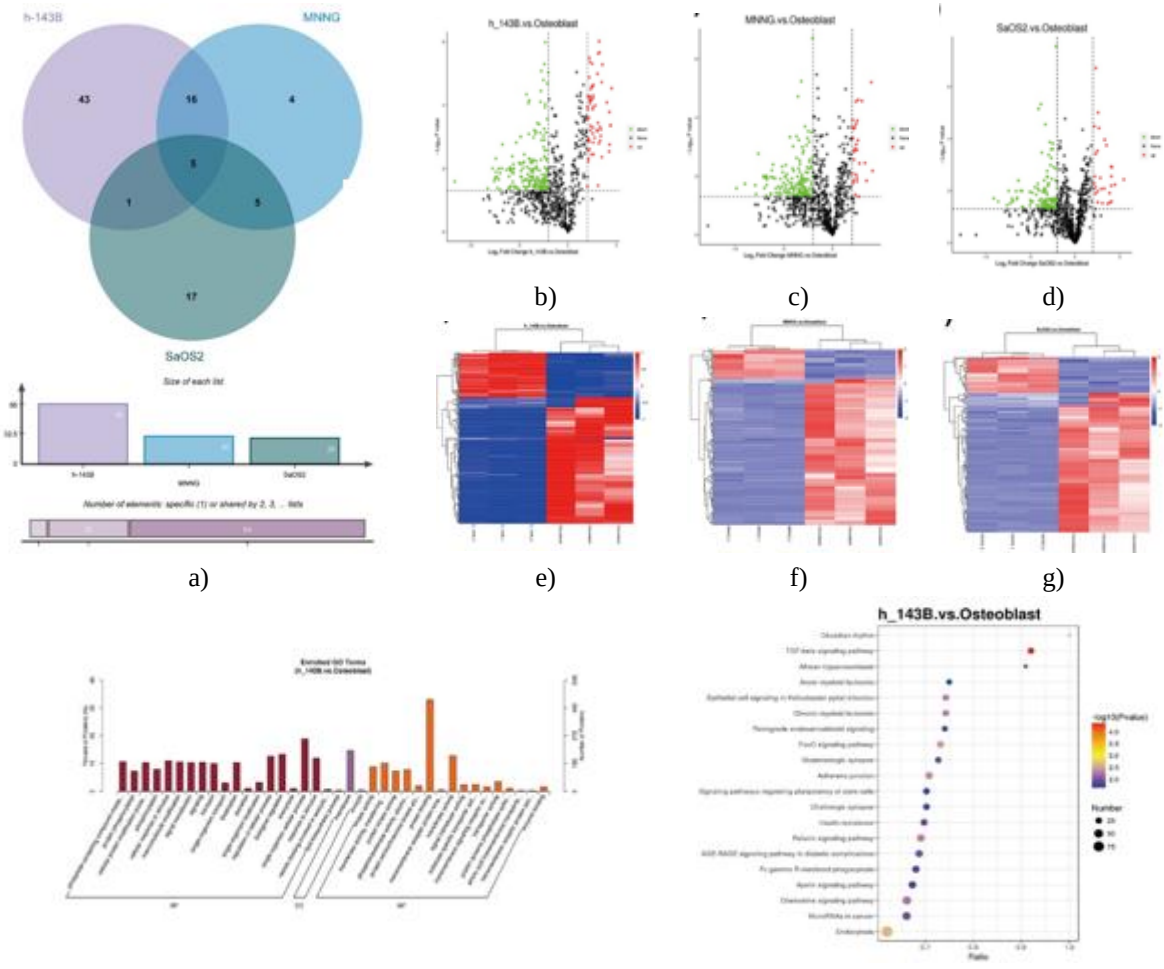

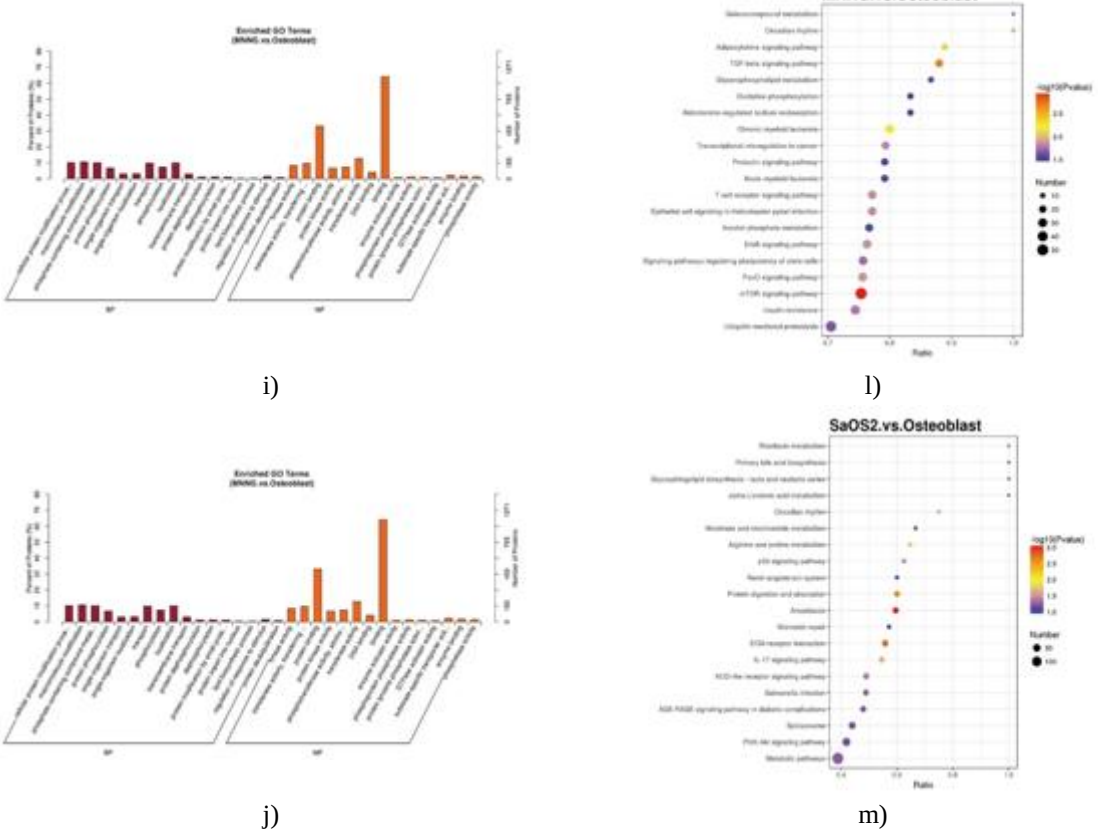

i) l)

j) m)

Figure 3. Detection of differentially expressed proteins (DEPs) in exosomes from osteoblasts versus OS cells and functional annotation through bioinformatics. (a) Venn diagram illustrating the overlap in exosomal proteomic profiles. Comparison of differentially expressed proteins across exosomes from various OS cell lines. (b–d) Volcano plots depicting differentially expressed proteins between osteoblasts and (b) 143B cells, (c) MNNG/HOS cells, (d) SaOS-2 cells. Green dots represent downregulated proteins, red dots indicate upregulated proteins, and black dots signify proteins without significant change. (e–g) Heatmaps showing differentially expressed proteins between osteoblasts and (e) 143B, (f) MNNG/HOS, (g) SaOS-2 cells as determined by DIA-based quantitative proteomics. (h–j) Bar graphs summarizing Gene Ontology (GO) classification of the DEPs. Results are grouped into three main categories: biological processes (BP), cellular components (CM), and molecular functions (MF). (k–m) Top 20 enriched KEGG pathways for DEPs in (k) 143B, (l) MNNG/HOS, and (m) SaOS-2 cells, respectively. BP, biological processes; CM, cellular components; DEPs, differential expressed proteins; DIA, data-independent acquisition; GO, gene ontology; KEGG, Kyoto Encyclopedia of Genes and Genomes; MF, molecular functions; OS, osteosarcoma.

GO enrichment and KEGG pathway analyses

Gene Ontology (GO) annotation was performed with Blast2GO software to assess the biological relevance of the differentially expressed proteins (DEPs). Subsequent GO enrichment analysis categorized these DEPs and generated functional classification charts illustrating both upregulated and downregulated proteins **(Figures 3b–3g)**. The resulting charts revealed that the DEPs participate in comparable structural and functional categories **(Figures 3h–3j)**. To gain deeper insight into the biological pathways influenced by these proteins, Kyoto Encyclopedia of Genes and Genomes (KEGG) pathway enrichment analysis was additionally conducted **(Figures 3k–3m)**.

Subcellular localization and protein–protein interaction network analysis

The subcellular distribution of the identified DEPs was predicted using WoLF PSORT software. The DEPs were then uploaded to the STRING database (version 11.0) for construction of a protein–protein interaction network, focusing on the top 100 interactions by confidence score.

YES1 is substantially overexpressed in OS cells and clinical OS specimens and is associated with unfavorable prognosis

YES1 was identified as a novel protein enriched in OS-derived exosomes through DIA-based proteomics, yet its functional significance in OS remains largely unexplored. Comparative DIA profiling of exosome-treated OS cell lines (Exo-MNNG/HOS, Exo-SaOS-2, Exo-143B) versus untreated controls demonstrated enrichment of several proteins, including YES1, within the tumor-derived exosomes **(Figures 3a–3g)**. The corresponding GO and KEGG analysis outcomes are presented in **Figures 3h–3m**. Venn diagram analysis of DEPs from MNNG/HOS, SaOS-2, and 143B cells confirmed consistent upregulation of YES1 across all three lines. This finding was validated by Western blotting of both whole-cell lysates and isolated exosomes **(Figures 4a and 4b)**.

To investigate the contribution of YES1 to OS pathogenesis, both overexpression and knockdown experiments were performed. Western blot analysis also verified successful modulation of YES1 levels in exosomes following transfection of MNNG/HOS and SaOS-2 cells **(Figure 4c)**. Further validation in clinical specimens was achieved through Western blotting, quantitative real-time polymerase chain reaction (qRT-PCR), and IHC. These analyses consistently showed markedly elevated YES1 protein and mRNA levels in OS tissues relative to adjacent non-tumorous tissues (n = 6 for protein analysis) **(Figure 4d)**. qRT-PCR confirmed higher YES1 mRNA expression in a larger cohort of OS tissues (n = 20) compared with non-tumor tissues (n = 20) **(Figure 4e)**, with IHC scoring aligning with these results **(Figure 4f)**.

The association between YES1 expression and clinicopathological features was evaluated in 44 OS patients **(Table 1)**. Elevated YES1 levels were significantly correlated with larger tumor size (> 3 cm²), but showed no statistically meaningful relationship with patient age, sex, tumor site, or metastatic status. Moreover, high YES1 expression was associated with reduced overall survival (p = 0.018) during the observation period **(Figure 4g)**. Representative IHC images illustrating YES1 staining patterns in OS patient samples are provided in **Figure 4f**.

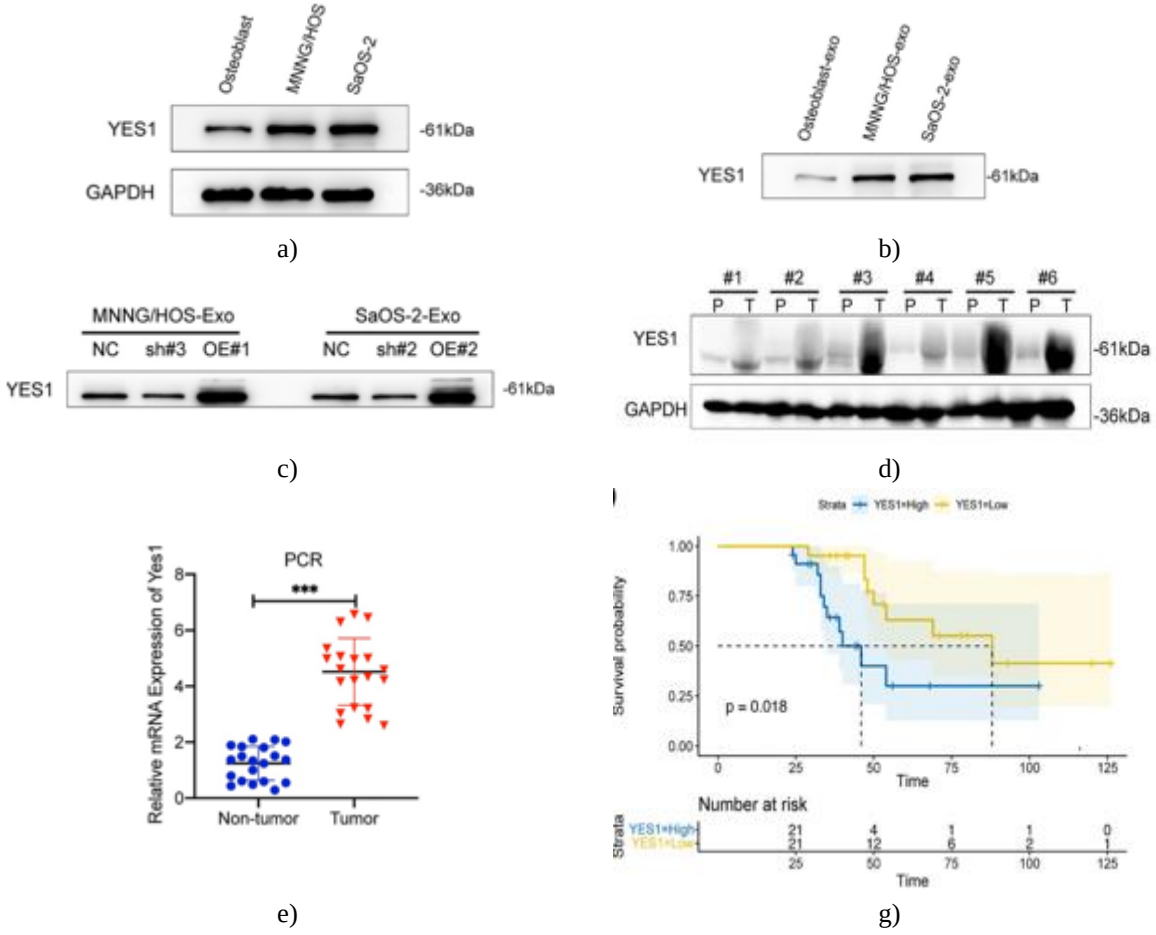

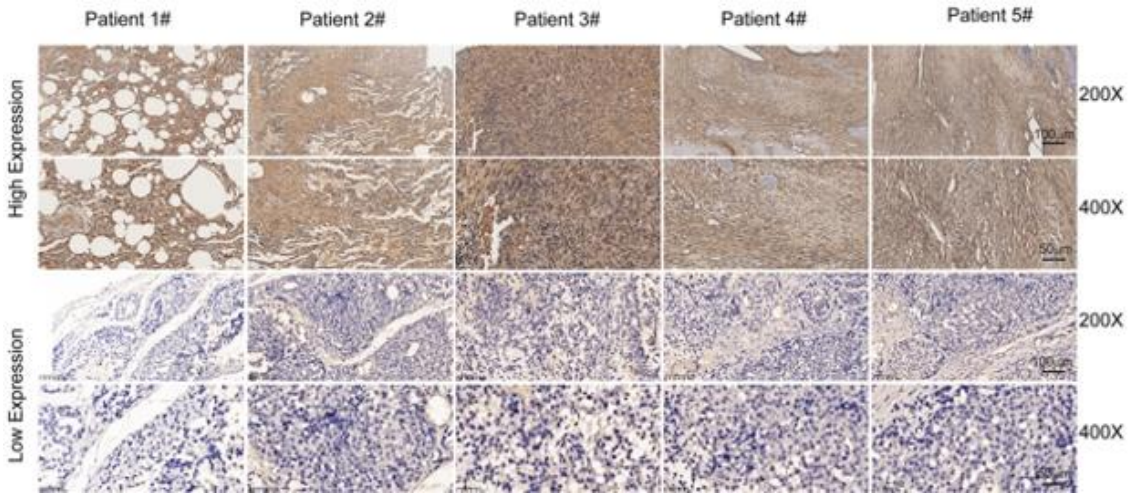

f)

Figure 4. Association of YES1 expression with clinical prognosis and immune features in OS patients. (a) Western blot analysis of YES1 protein levels in OS cell lines. (b) Western blot detection of YES1 in exosomes derived from OS cells. (c) Western blot examination of YES1 expression in OS cells and their derived exosomes following treatment with cancer cell-derived exosomes. (d) Western blot analysis of YES1 protein abundance in OS tissues. (e) Quantitative PCR assessment of YES1 mRNA expression in OS patient tissues (n = 20). (f) Representative immunohistochemical images showing YES1 expression in OS tissues from patients. Scale bar, 100 μm, 50 μm. (g) Kaplan–Meier survival curves comparing overall survival according to YES1 expression levels. OS, osteosarcoma; qPCR, quantitative polymerase chain reaction.

Table 1. Clinicopathological features of 44 patients diagnosed with osteosarcoma.

Variable	Low YES1 expression (n=21)	High YES1 expression (n=23)	p-value
Total number	21	23	—
Gender			p = 0.232
Male	12	9	
Female	9	14	
Age (years)	21.29 ± 8.70 (8–40)	20.13 ± 7.99 (9–42)	p = 0.648
Tumor location			p = 0.992
Femur	12	14	
Tibia	7	6	
Other sites	2	3	
Presence of lung metastasis			p = 0.006
No	16	8	
Yes	5	15	
Follow-up duration (months)	62.43 ± 26.64 (29–126)	40.61 ± 17.31 (24–103)	p = 0.002
Eneking stage			p < 0.001
Stage I	12	1	
Stage II	9	6	
Stage III	0	16	
Tumor size			p < 0.001
< 3 cm	17	5	
> 3 cm	4	18	
Patient status			p = 0.190
Survived	15	12	
Deceased	6	11	

YES1 expression across multiple cancer types and its prognostic implications from TCGA data

Prior studies have implicated YES1 in cancer progression and metastatic spread in several malignancies. To extend these observations, comprehensive bioinformatic evaluations were undertaken. Examination of YES1 transcript levels in tumor and matched normal tissues via the TCGA database indicated marked upregulation of

YES1 in numerous cancer types relative to their normal counterparts. Furthermore, survival analyses across cancer cohorts demonstrated that patients displaying elevated YES1 expression experienced significantly inferior clinical outcomes compared with those showing lower expression. Additional investigations assessed potential links between YES1 levels and immune cell infiltration within the pan-cancer setting, aiming to clarify its influence on the tumor immune landscape. Results revealed strong positive associations between heightened YES1 expression and greater infiltration by diverse immune cell populations. YES1 expression also correlated positively with tumor mutational burden (TMB) and microsatellite instability (MSI), with higher YES1 levels corresponding to elevated TMB and MSI scores ($p < 0.05$). Immunosuppressive agent sensitivity profiling further uncovered differential responses between cohorts stratified by high versus low YES1 expression.

Exosomal YES1 drives osteosarcoma cell proliferation, migration, and invasion by activating the MAPK cascade

It was postulated that YES1 facilitates osteosarcoma (OS) cell proliferation, migration, and invasive behavior chiefly by stimulating ERK phosphorylation (p-ERK) in the MAPK pathway. Overexpression of YES1 (OE YES1) led to pronounced increases in p-ERK and p-MEK, alongside reductions in p-p38 and p-JNK. These alterations were intensified by co-treatment with tumor-derived exosomes and could be abrogated using the ERK inhibitor U0126 or the broader MAPK inhibitor SB-203580, establishing ERK as a critical downstream target of YES1. By contrast, YES1 knockdown (shYES1) resulted in substantial downregulation of p-ERK and p-MEK with concurrent upregulation of p-p38 and p-JNK. Addition of exosomes partially reversed these shifts by elevating p-ERK and p-MEK while lowering p-p38 and p-JNK **(Figures 5a–5d)**. Such rescue was strengthened by ERK pathway agonists EGF and IL-1β, supporting the regulatory function of YES1 and its exosomal form in MAPK pathway dynamics. These signaling changes aligned with functional outcomes. shYES1 cells exhibited clear deficits in proliferative, migratory, and invasive capacities, as quantified by EdU, wound healing, and Transwell assays. Exosome supplementation partly restored these functions, and EGF administration produced further improvement, confirming the relevance of ERK signaling **(Figures 6a–6d)**. Annexin V/PI flow cytometry additionally showed elevated apoptosis following YES1 depletion, an effect that was partially countered by exosomes and more fully reversed by EGF **(Figure 6b)**. In parallel, YES1 overexpression enhanced proliferative, migratory, and invasive phenotypes, with exosomes exerting synergistic reinforcement. EGF treatment amplified these oncogenic properties, further validating ERK activation as a key mediator of YES1-driven tumor progression.

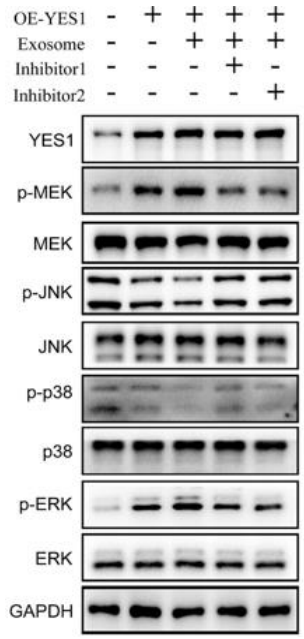

a)

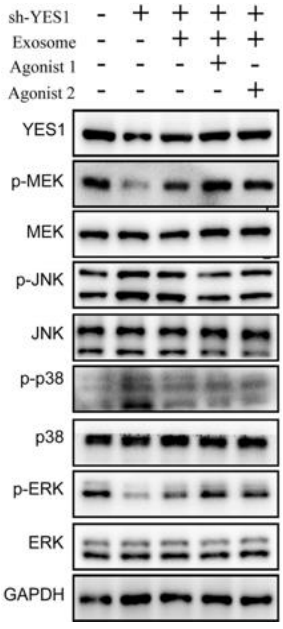

b)

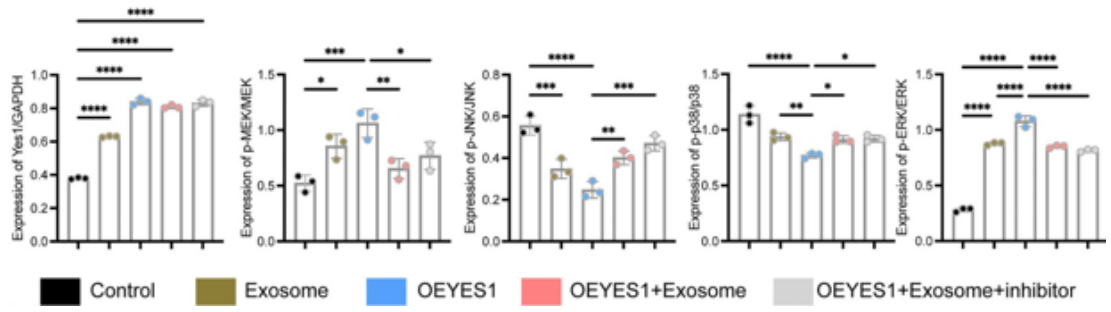

c)

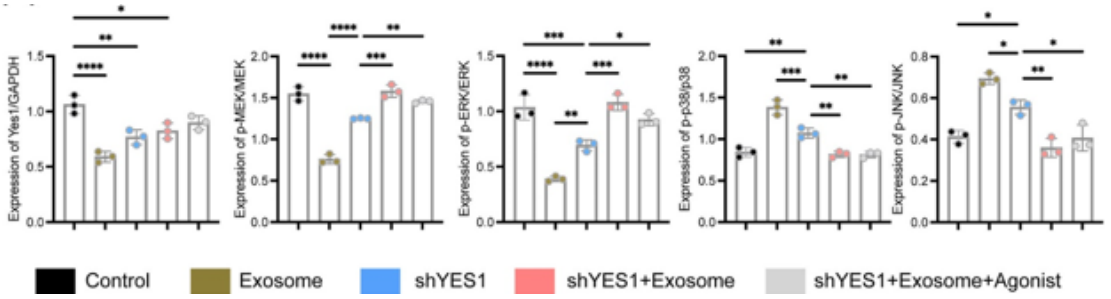

d)

Figure 5. YES1 potentially promotes OS proliferation, migration, and invasion by modulating ERK signaling. (a) OS cells received treatments with or without OS cell-derived exosomes combined with shYES1 transfection and the presence or absence of pathway inhibitors, followed by immunoblot analysis of MAPK components (phosphorylation status of MEK, p38, ERK, and JNK). (b) OS cells were exposed to OS cell-derived exosomes or vehicle, YES1 overexpression, and agonists or controls, after which MAPK pathway activation (phosphorylation of MEK, p38, ERK, and JNK) was assessed by immunoblotting. (c, d) Densitometric quantification of MAPK-related proteins in OS cells. Data represent the mean ± SD of three independent replicates. (*p < 0.05, **p < 0.01, ***p < 0.001). OS, osteosarcoma.

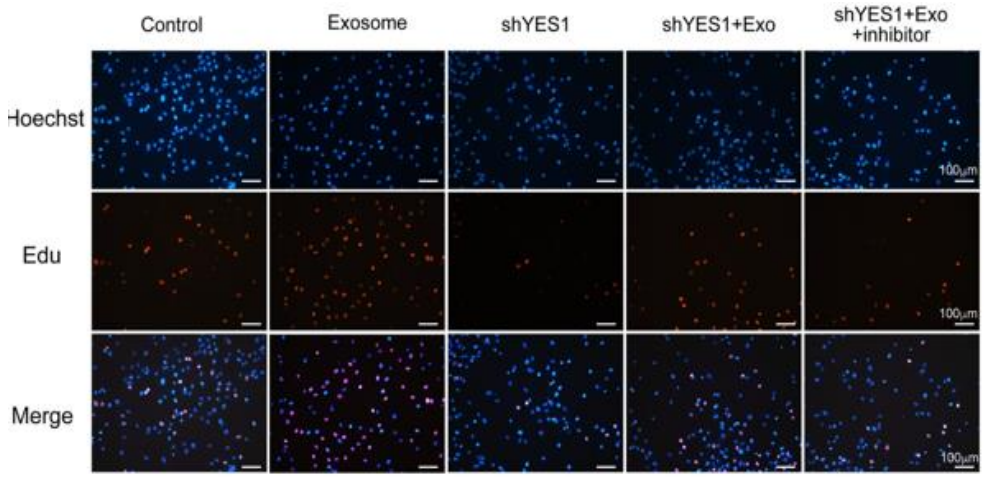

a)

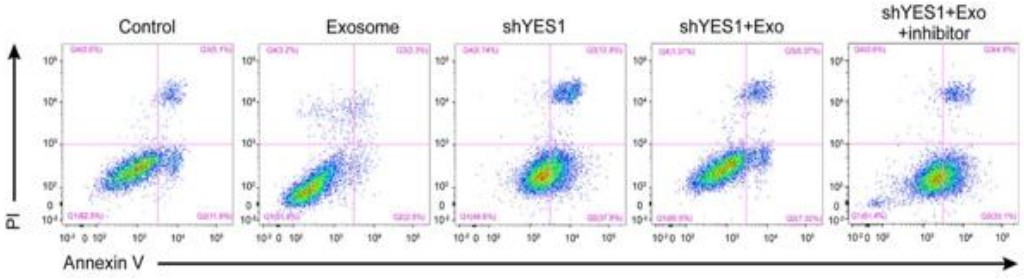

b)

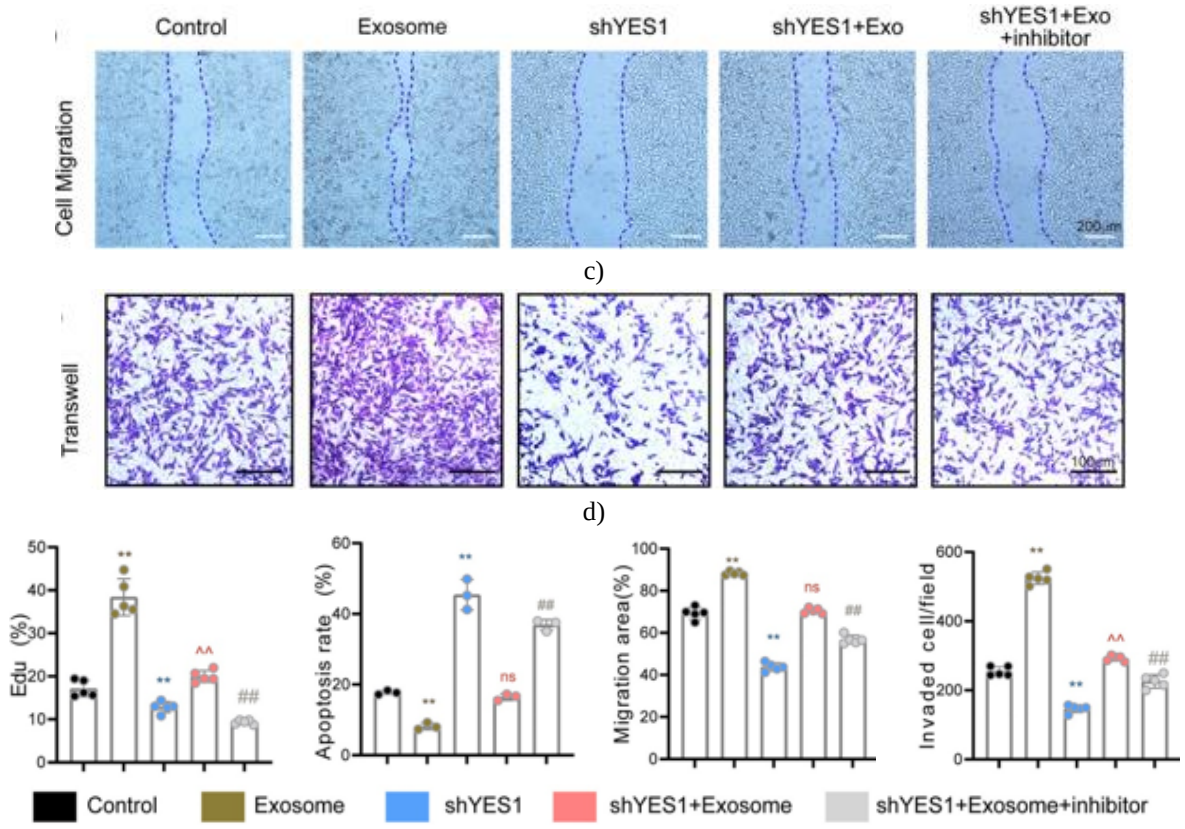

Figure 6. (a) Proliferative activity was measured by EdU assay in OS cells treated with or without OS cell-derived exosomes, shYES1, and inhibitor as indicated. Scale bar, 200 μm. (b) Apoptosis rates in OS cells were determined via Annexin V/PI staining and flow cytometry. (c) Representative wound healing images captured at 0 h and 24 h; dotted lines delineate scratch boundaries for each experimental condition. Scale bar, 200 μm. (d) Migration and invasion capacities were evaluated using standard or Matrigel-coated Transwell chambers in OS cells. Scale bar, 200 μm. (e) Percentage of EdU-positive OS cells (n = 5). (f) Mean apoptosis rate (%) in OS cells (n = 3). (g) Quantification of wound closure percentage in OS cells (n = 5). (h) Quantification of migrated or invaded cells (n = 5). OS, osteosarcoma. Symbols **, ##, and ^^ indicate $p < 0.05$ versus the respective control group.

Utilizing a subcutaneous xenograft model in nude mice, the impact on tumor development and dissemination was examined in five cohorts: control, shYES1, exosome supplementation, shYES1 plus exosomes, and shYES1 plus exosomes with inhibitor. In vivo bioluminescence imaging showed markedly diminished tumor burden and metastatic burden in shYES1 tumors relative to controls, while exosome delivery partially reinstated growth and spread. Inhibitor co-administration in the shYES1 + exosome group potently restrained progression, demonstrating that ERK signaling is integral to the pro-tumorigenic activity of exosomal YES1. Supporting histological data were obtained. HE-stained sections displayed reduced tumor size and proliferative regions in the shYES1 condition, partially reversed by exosomes. The shYES1 + exosome + inhibitor group presented the least aggressive histology, with smaller tumor nodules and lower cell density. PCNA immunostaining verified decreased proliferation in shYES1 tumors, partial recovery with exosomes, and renewed suppression upon inhibitor exposure. TUNEL assays detected heightened apoptosis in shYES1 tumors compared with controls; exosomes lowered apoptosis levels, while inhibitor treatment restored them, aligning with ERK pathway inhibition. These differences reached statistical significance ($p < 0.05$), underscoring the essential contributions of YES1 and exosomal YES1 to the regulation of tumor cell proliferation and survival through ERK-mediated signaling **(Figures 7a and 7b)**.

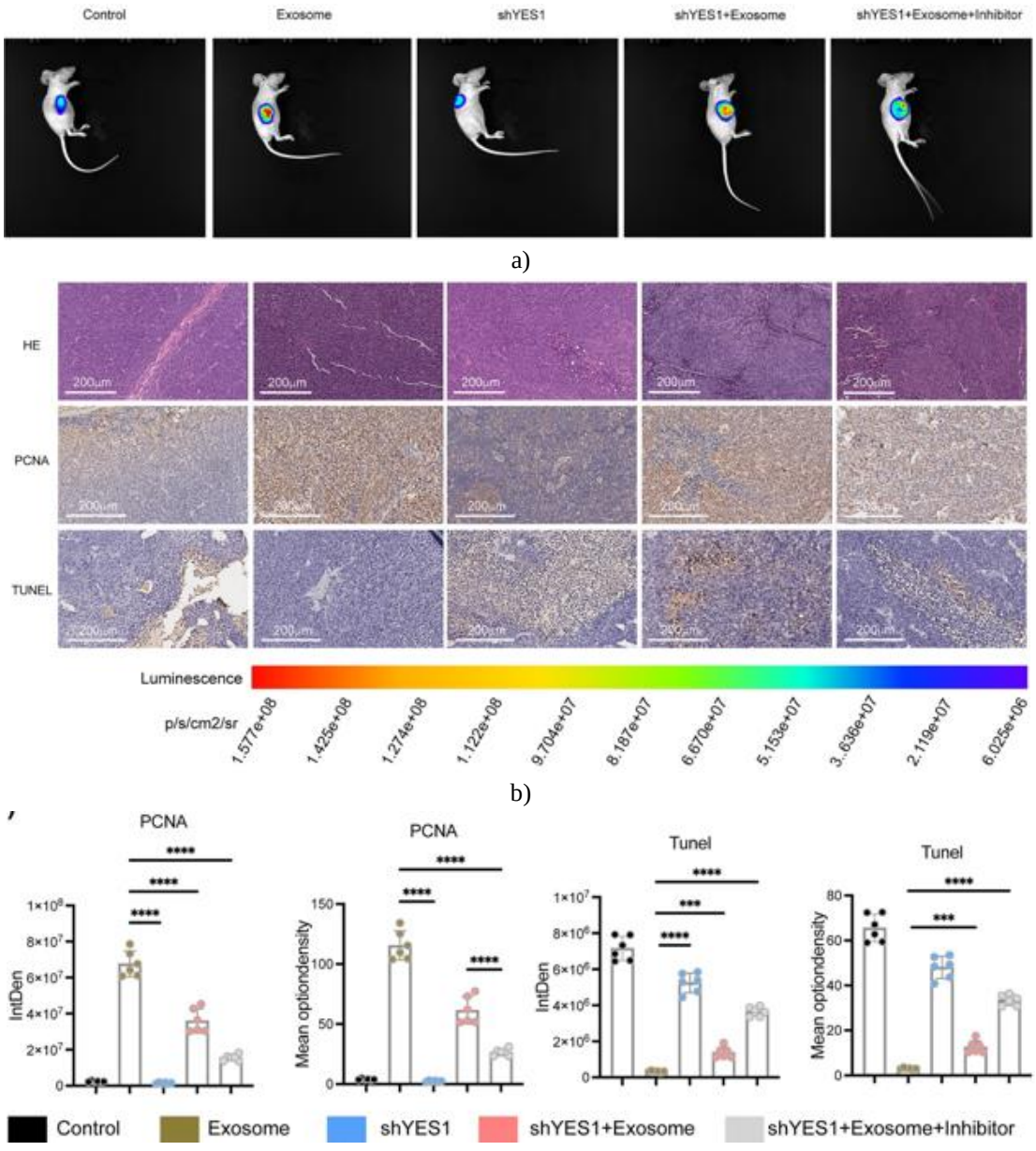

Figure 7. Representative images of subcutaneous tumors in nude mice inoculated with control or exosome-treated MNNG/HOS cells (n = 6 per group). (a) Tumor progression was tracked by bioluminescence imaging with an in vivo imaging system. (b) Representative HE staining, PCNA immunohistochemistry, and TUNEL assay images. Scale bar: 200 μm. (c) Quantitative analysis of PCNA and TUNEL staining. IHC, immunohistochemistry; PCNA, proliferating cell nuclear antigen; TUNEL, terminal deoxynucleotidyl transferase-mediated dUTP-biotin nick end labeling. : *p < 0.05; : **p < 0.01; : ***p < 0.001; : ****p < 0.0001.

YES1 May facilitate OS tumorigenesis through modulation of immune cell infiltration in the tumor microenvironment

Bioinformatic examination of YES1 across patients with diverse cancer types uncovered a notable association between YES1 expression and multiple malignancies. In particular, elevated YES1 levels were associated with enhanced infiltration of various immune cell populations. Application of six established immune deconvolution algorithms to assess the relationship between YES1 expression and immune cell abundance demonstrated that individuals with higher YES1 expression exhibited substantially greater immune cell infiltration, especially T cells, in multiple cancer types relative to those with lower expression. In addition, significant differences in immunomodulatory molecule expression were identified between the high and low YES1 expression groups,

indicating that YES1 contributes importantly to remodeling of the tumor microenvironment (TME). Correlation analyses involving immune checkpoint genes further reinforced the notion that YES1 exerts a substantial influence on immune regulation within the TME. To corroborate these computational observations at the protein level, multiplex immunohistochemistry (mIHC) was conducted on OS clinical specimens. Specific markers for YES1, T cell subsets (CD4 and FoxP3), and PD-L1 were simultaneously visualized through multi-color fluorescence imaging. The staining patterns confirmed co-localization of YES1 with immune cell infiltrates, aligning closely with the predicted cellular distributions **(Figure 8a)**. Overall, YES1 expression correlated strongly with increased immune cell presence in OS tumor tissues compared with adjacent non-tumorous tissues. Notably, PD-L1 protein expression detected by mIHC was consistent with the bioinformatic predictions, thereby strengthening evidence for the involvement of YES1 in immune modulation within the TME. A schematic diagram integrating the principal findings of this study is provided in **Figure 8b**, offering a unified view of the proposed mechanistic pathway and its broader significance.

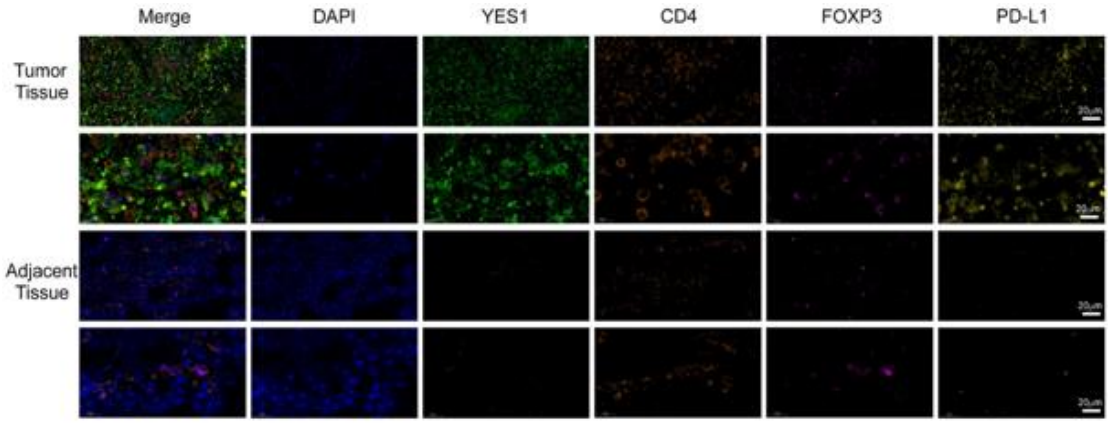

a)

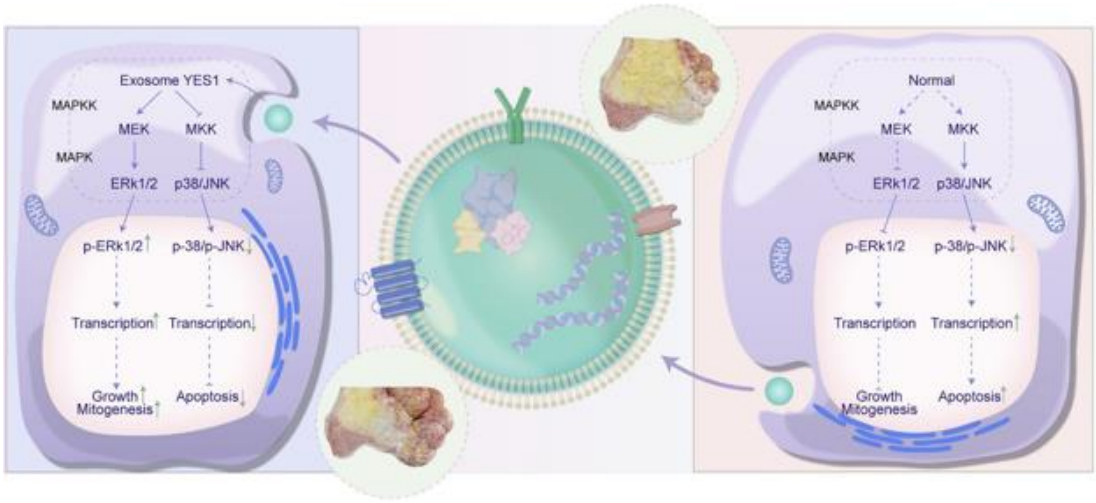

b)

Figure 8. Immune cell infiltration assessed at the protein level within the tumor microenvironment. (a) Representative multiplex immunohistochemistry images showing expression of YES1, CD4, FoxP3, and PD-L1 in OS patient tissues. Scale bar, 100 μm. (b) Exosomal YES1 exerts an oncogenic function in OS progression through the MAPK pathway. OS, osteosarcoma.

Osteosarcoma (OS) is recognized as a highly aggressive primary bone malignancy. Patients undergoing surgery as the sole intervention historically exhibit a survival rate of only 15%–17% [27, 28]. The incorporation of adjuvant chemotherapy alongside surgical resection has substantially improved the 5-year overall survival rate to approximately 70%. Nevertheless, outcomes for individuals with metastatic or recurrent disease have shown minimal improvement over the past three decades, remaining at roughly 20% for 5-year survival [29].

Consequently, elucidating the molecular mechanisms driving OS and identifying innovative therapeutic targets remain critical priorities.

Intercellular communication plays a fundamental role in tumor development and metastatic dissemination. Exosomes function as key mediators in these interactions, modulating signaling cascades across various physiological and pathological states [30, 31]. Virtually all cell types release exosomes; however, those secreted by cancer cells are typically more abundant than those from normal cells and are closely linked to oncogenesis and malignant progression [7, 32]. A substantial body of evidence indicates that tumor-derived exosomes contribute to cancer advancement by remodeling the tumor microenvironment through the transfer of bioactive molecules, including proteins and RNAs, between cells [33-35]. Proteomic profiling of exosomes isolated from human OS cells and osteoblasts offers valuable insights into the underlying biological processes of this malignancy. Numerous investigations have established exosomal proteins as promising diagnostic, prognostic, and therapeutic biomarkers. Comparative secretome analyses between malignant and non-malignant cells have successfully identified tumor-associated markers in multiple malignancies, such as prostate, lung, breast, ovarian, and other cancers [36, 37].

In the present study, exosomes derived from osteoblasts and OS cells were thoroughly characterized using transmission electron microscopy (TEM), western blotting, and nanoparticle tracking analysis (NTA). TEM imaging demonstrated the typical cup-shaped morphology, NTA verified particle sizes consistent with the expected exosomal range, and western blotting confirmed marked enrichment of canonical exosomal markers—including Alix, TSG101, HSP70, and CD9—relative to their parental cells [30, 38]. This selective packaging of proteins is attributed to specific biogenesis pathways that concentrate particular molecules to support exosome architecture and facilitate efficient intercellular signaling. Uptake experiments employing DiO-labeled exosomes (green fluorescence), combined with DAPI nuclear staining (blue) and phalloidin cytoskeletal labeling (red), verified internalization by OS cells. The observed time-dependent accumulation further supports active endocytosis, highlighting the dynamic nature of exosome transfer and its potential influence on cellular phenotypes within the tumor microenvironment. Functional assays revealed that OS cell-derived exosomes markedly enhanced proliferation, migration, and invasion of OS cells both in vitro and in vivo. These effects were confirmed by increased EdU incorporation, reduced apoptotic rates in flow cytometry, and accelerated wound closure and Transwell migration/invasion. In xenograft models, administration of exosome-pretreated MNNG/HOS cells led to accelerated tumor growth in nude mice, accompanied by elevated PCNA levels and diminished TUNEL-positive cells, indicating that exosomal cargo enriched with stable proteins actively drives OS tumorigenesis. To pinpoint key functional components within these exosomes, data-independent acquisition (DIA) proteomic analysis was performed to screen for candidate biomarkers, followed by detailed functional and mechanistic studies in the context of OS progression [39, 40].

YES proto-oncogene 1 (YES1), a member of the Src family of non-receptor tyrosine kinases, encodes a protein implicated in various pathologies, including sarcoma and megaesophagus [41]. While c-Src has been extensively investigated in relation to drug resistance, and several Src family kinase inhibitors have been evaluated across cancer types, knowledge regarding YES1 function in OS remains limited [42]. Prior research has linked YES1 amplification to acquired resistance against targeted therapies in breast cancer [43] and to evasion of 5-fluorouracil-induced apoptosis in colorectal cancer [44]. The current investigation demonstrates that exosomal YES1 contributes significantly to OS progression and that elevated YES1 protein expression correlates with poorer overall survival in OS patients.

Bioinformatic analysis indicated that YES1 is overexpressed across multiple tumor types and functions as a proto-oncogene. Analysis of TCGA datasets demonstrated that elevated YES1 expression is significantly associated with reduced overall survival and disease-specific survival in pan-cancer cohorts relative to normal tissues. Correlation studies further revealed a robust relationship between YES1 levels and immune cell infiltration, with the strongest associations observed for T cells. In addition, YES1 expression showed positive correlations with several immune checkpoint molecules. Tumor mutational burden (TMB) and microsatellite instability were also linked to therapeutic responses, particularly to immune checkpoint blockade, implying that YES1 may represent a valuable biomarker for predicting immunotherapy efficacy. These computational observations were experimentally validated through Western blotting and immunohistochemistry on clinical tissue samples to confirm YES1 expression patterns. The interplay between YES1 overexpression and the tumor immune microenvironment, including potential interactions with other genetic alterations, was also examined. The experimental data aligned closely with bioinformatic predictions, confirming that heightened YES1 expression is

strongly associated with unfavorable prognosis and shorter overall survival. Notably, increased YES1 levels corresponded with greater infiltration of $CD4^+/FOXP3^+$ regulatory T cells (Tregs), which promote an immunosuppressive environment in osteosarcoma.

The mitogen-activated protein kinase (MAPK) signaling cascade, encompassing ERK, JNK, and p38 branches, regulates critical cellular functions including proliferation, differentiation, apoptosis, and responses to stress, and is commonly altered in malignant diseases. Among these, ERK signaling is frequently hyperactivated in cancers, promoting sustained cell growth and survival through regulation of oncogenic transcription factors and suppression of apoptotic pathways [45, 46]. The present study demonstrates that YES1, particularly when delivered via exosomes, primarily stimulates the ERK pathway in osteosarcoma cells, thereby enhancing tumor cell proliferation, migration, and invasion. Western blot results showed that YES1 overexpression increased phosphorylation of ERK and MEK while decreasing phosphorylation of p38 and JNK, without affecting the total protein levels of MEK, p38, JNK, or ERK. This pattern suggests that exosomal YES1 selectively potentiates the ERK arm of MAPK signaling while attenuating stress-responsive branches. Complementary functional experiments and animal models reinforced these molecular findings: exposure to exosomes promoted aggressive tumorigenic phenotypes in OS cells, whereas YES1 depletion markedly attenuated these effects. Pharmacological modulation of ERK activity either rescued or further suppressed the observed phenotypes. Taken together, these data illustrate that exosomal YES1 drives osteosarcoma progression predominantly through targeted activation of ERK signaling within the MAPK network, while concurrent modulation of p38 and JNK pathways may support tumor adaptation, survival, and metastatic spread.

Conclusion

This investigation establishes exosomal YES1 as a significant oncogenic driver in osteosarcoma that operates primarily through the MAPK signaling pathway, highlighting its promise as a novel diagnostic and therapeutic target. Comprehensive in vitro and in vivo analyses provide fresh insights into the contribution of YES1 to osteosarcoma progression and open potential new directions for clinical intervention. Subsequent studies will focus on further elucidating the specific contributions of OS-derived exosomal YES1 with the goal of advancing its translational application in osteosarcoma management.

Acknowledgments: None

Conflict of Interest: None

Financial Support: None

Ethics Statement: None

References

1. Kelley LM, Schlegel M, Hecker-Nolting S, Kevric M, Haller B, Rössig C, et al. Pathological fracture and prognosis of high-grade osteosarcoma of the extremities: an analysis of 2,847 consecutive Cooperative Osteosarcoma Study Group (COSS) patients. J Clin Oncol. 2020;38(8):823-33. doi:10.1200/JCO.19.00827
2. Bielack SS, Kempf-Bielack B, Delling G, Exner GU, Flege S, Helmke K, et al. Prognostic factors in high-grade osteosarcoma of the extremities or trunk: an analysis of 1,702 patients treated on neoadjuvant Cooperative Osteosarcoma Study Group protocols. J Clin Oncol. 2002;20(3):776-90. doi:10.1200/JCO.2002.20.3.776
3. Isakoff MS, Bielack SS, Meltzer P, Gorlick R. Osteosarcoma: current treatment and a collaborative pathway to success. J Clin Oncol. 2015;33(27):3029-35. doi:10.1200/JCO.2014.59.4895
4. Luetke A, Meyers PA, Lewis I, Juergens H. Osteosarcoma treatment - where do we stand? A state of the art review. Cancer Treat Rev. 2014;40(4):523-32. doi:10.1016/j.ctrv.2013.11.006
5. Steinbichler TB, Dudás J, Riechelmann H, Skvortsova II. The role of exosomes in cancer metastasis. Semin Cancer Biol. 2017;44:170-81. doi:10.1016/j.semcancer.2017.02.006

6. Maacha S, Bhat AA, Jimenez L, Raza A, Haris M, Uddin S, et al. Extracellular vesicles-mediated intercellular communication: roles in the tumor microenvironment and anti-cancer drug resistance. Mol Cancer. 2019;18(1):55. doi:10.1186/s12943-019-0965-7
7. Kalluri R, LeBleu VS. The biology, function, and biomedical applications of exosomes. Science. 2020;367(6478):eaau6977. doi:10.1126/science.aau6977
8. Kalluri R. The biology and function of exosomes in cancer. J Clin Invest. 2016;126(4):1208-15. doi:10.1172/JCI81135
9. Maas SLN, Breakefield XO, Weaver AM. Extracellular vesicles: unique intercellular delivery vehicles. Trends Cell Biol. 2017;27(3):172-88. doi:10.1016/j.tcb.2016.11.003
10. Xu R, Greening DW, Zhu HJ, Takahashi N, Simpson RJ. Extracellular vesicle isolation and characterization: toward clinical application. J Clin Invest. 2016;126(4):1152-62. doi:10.1172/JCI81129
11. Pegtel DM, Gould SJ. Exosomes. Annu Rev Biochem. 2019;88:487-514. doi:10.1146/annurev-biochem-013118-111902
12. Mashouri L, Yousefi H, Aref AR, Ahadi AM, Molaei F, Alahari SK. Exosomes: composition, biogenesis, and mechanisms in cancer metastasis and drug resistance. Mol Cancer. 2019;18(1):75. doi:10.1186/s12943-019-0991-5
13. Wu M, Wang G, Hu W, Yao Y, Yu XF. Emerging roles and therapeutic value of exosomes in cancer metastasis. Mol Cancer. 2019;18(1):53. doi:10.1186/s12943-019-0964-8
14. Casey SC, Amedei A, Aquilano K, Azmi AS, Benencia F, Bhakta D, et al. Cancer prevention and therapy through the modulation of the tumor microenvironment. Semin Cancer Biol. 2015;35 Suppl:S199-223. doi:10.1016/j.semcancer.2015.02.007
15. Whiteside TL. Exosomes and tumor-mediated immune suppression. J Clin Invest. 2016;126(4):1216-23. doi:10.1172/JCI81136
16. Mallick P, Kuster B. Proteomics: a pragmatic perspective. Nat Biotechnol. 2010;28(7):695-709. doi:10.1038/nbt.1658
17. Geyer PE, Holdt LM, Teupser D, Mann M. Revisiting biomarker discovery by plasma proteomics. Mol Syst Biol. 2017;13(9):942. doi:10.15252/msb.20156297
18. Huang Z, Ma L, Huang C, Li Q, Nice EC. Proteomic profiling of human plasma for cancer biomarker discovery. Proteomics. 2017;17(6). doi:10.1002/pmic.201600240
19. Hoshino A, Kim HS, Bojmar L, Gyan KE, Cioffi M, Hernandez J, et al. Extracellular vesicle and particle biomarkers define multiple human cancers. Cell. 2020;182(4):1044-61. doi:10.1016/j.cell.2020.07.009
20. Garmendia I, Pajares MJ, Hermida-Prado F, Ajona D, Bértolo C, Sainz C, et al. YES1 drives lung cancer growth and progression and predicts sensitivity to dasatinib. Am J Respir Crit Care Med. 2019;200(7):888-99. doi:10.1164/rccm.201807-1292OC
21. Pang Y, Liu Z, Han H, Wang B, Li W, Mao C, et al. Peptide SMIM30 promotes HCC development by inducing SRC/YES1 membrane anchoring and MAPK pathway activation. J Hepatol. 2020;73(5):1155-69. doi:10.1016/j.jhep.2020.05.028
22. Fang Z, Yin S, Sun R, Zhang S, Fu M, Wu Y, et al. miR-140-5p suppresses the proliferation, migration and invasion of gastric cancer by regulating YES1. Mol Cancer. 2017;16(1):139. doi:10.1186/s12943-017-0708-6
23. Cox J, Mann M. MaxQuant enables high peptide identification rates, individualized p.p.b.-range mass accuracies and proteome-wide protein quantification. Nat Biotechnol. 2008;26(12):1367-72. doi:10.1038/nbt.1511
24. Bruderer R, Bernhardt OM, Gandhi T, Reiter L. High-precision iRT prediction in the targeted analysis of data-independent acquisition and its impact on identification and quantitation. Proteomics. 2016;16(15-16):2246-56. doi:10.1002/pmic.201500488
25. Jones P, Binns D, Chang HY, Fraser M, Li W, McAnulla C, et al. InterProScan 5: genome-scale protein function classification. Bioinformatics. 2014;30(9):1236-40. doi:10.1093/bioinformatics/btu031
26. Huang DW, Sherman BT, Lempicki RA. Systematic and integrative analysis of large gene lists using DAVID bioinformatics resources. Nat Protoc. 2009;4(1):44-57. doi:10.1038/nprot.2008.211
27. Bernthal NM, Federman N, Eilber FR, Nelson SD, Eckardt JJ, Eilber FC, et al. Long-term results (>25 years) of a randomized, prospective clinical trial evaluating chemotherapy in patients with high-grade, operable osteosarcoma. Cancer. 2012;118(23):5888-93. doi:10.1002/cncr.27651

28. Link MP, Goorin AM, Miser AW, Green AA, Pratt CB, Belasco JB, et al. The effect of adjuvant chemotherapy on relapse-free survival in patients with osteosarcoma of the extremity. N Engl J Med. 1986;314(25):1600-6. doi:10.1056/NEJM198606193142502
29. Meyers PA, Healey JH, Chou AJ, Wexler LH, Merola PR, Morris CD, et al. Addition of pamidronate to chemotherapy for the treatment of osteosarcoma. Cancer. 2011;117(8):1736-44. doi:10.1002/cncr.25744
30. Ruivo CF, Adem B, Silva M, Melo SA. The biology of cancer exosomes: insights and new perspectives. Cancer Res. 2017;77(23):6480-8. doi:10.1158/0008-5472.CAN-17-0994
31. Shen M, Ren X. New insights into the biological impacts of immune cell-derived exosomes within the tumor environment. Cancer Lett. 2018;431:115-22. doi:10.1016/j.canlet.2018.05.038
32. Peinado H, Alečković M, Lavotshkin S, Matei I, Costa-Silva B, Moreno-Bueno G, et al. Melanoma exosomes educate bone marrow progenitor cells toward a pro-metastatic phenotype through MET. Nat Med. 2012;18(6):883-91. doi:10.1038/nm.2753
33. Lu M, Huang B, Hanash SM, Onuchic JN, Ben-Jacob E. Modeling putative therapeutic implications of exosome exchange between tumor and immune cells. Proc Natl Acad Sci U S A. 2014;111(40):E4165-74. doi:10.1073/pnas.1416745111
34. Hu W, Liu C, Bi ZY, Zhou Q, Zhang H, Li LL, et al. Comprehensive landscape of extracellular vesicle-derived RNAs in cancer initiation, progression, metastasis and cancer immunology. Mol Cancer. 2020;19(1):102. doi:10.1186/s12943-020-01199-1
35. Yang X, Zhang Y, Zhang Y, Zhang S, Qiu L, Zhuang Z, et al. The key role of exosomes on the pre-metastatic niche formation in tumors. Front Mol Biosci. 2021;8:703640. doi:10.3389/fmolb.2021.703640
36. Sardana G, Jung K, Stephan C, Diamandis EP. Proteomic analysis of conditioned media from the PC3, LNCaP, and 22Rv1 prostate cancer cell lines: Discovery and validation of candidate prostate cancer biomarkers. J Proteome Res. 2008;7(8):3329-38.
37. Sceneay J, Smyth MJ, Möller A. The pre-metastatic niche: Finding common ground. Cancer Metastasis Rev. 2013;32(3-4):449-64.
38. Zhu L, Sun HT, Wang S, Huang SL, Zheng Y, Wang CQ, et al. Isolation and characterization of exosomes for cancer research. J Hematol Oncol. 2020;13(1):152.
39. Jia B, Zhao X, Wu D, Dong Z, Chi Y, Zhao J, et al. Identification of serum biomarkers to predict pemetrexed/platinum chemotherapy efficacy for advanced lung adenocarcinoma patients by data-independent acquisition (DIA) mass spectrometry analysis with parallel reaction monitoring (PRM) verification. Transl Lung Cancer Res. 2021;10(2):981-94.
40. Rauniyar N. Parallel reaction monitoring: A targeted experiment performed using high resolution and high mass accuracy mass spectrometry. Int J Mol Sci. 2015;16(12):28566-81.
41. Silverman GA, Kuo WL, Taillon-Miller P, Gray JW. Chromosomal reassignment: YACs containing both YES1 and thymidylate synthase map to the short arm of chromosome 18. Genomics. 1993;15(2):442-5.
42. Lian I, Kim J, Okazawa H, Zhao J, Zhao B, Yu J, et al. The role of YAP transcription coactivator in regulating stem cell self-renewal and differentiation. Genes Dev. 2010;24(11):1106-18.
43. Wang L, Wang Q, Xu P, Fu L, Li Y, Fu H, et al. YES1 amplification confers trastuzumab–emtansine (T-DM1) resistance in HER2-positive cancer. Br J Cancer. 2020;123:1000-11.
44. Touil Y, Igoudjil W, Corvaisier M, Dessein AF, Vandomme J, Monté D, et al. Colon cancer cells escape 5FU chemotherapy-induced cell death by entering stemness and quiescence associated with the c-Yes/YAP axis. Clin Cancer Res. 2014;20(4):837-46.
45. Samatar AA, Poulikakos PI. Targeting RAS-ERK signalling in cancer: Promises and challenges. Nat Rev Drug Discov. 2014;13(12):928-42.
46. Yuan J, Dong X, Yap J, Hu J. The MAPK and AMPK signalings: Interplay and implication in targeted cancer therapy. J Hematol Oncol. 2020;13(1):113.